Iranian Journal of Catalysis 10(1), 2020, 33-45

IRANIAN JOURNAL OF CATALYSIS

Thermal regeneration and decoking optimization of chlorinated platinum/alumina catalysts for the isomerization process

Hamed Abbasi*

Chemistry and Chemical Engineering Research Center of Iran, Tehran, Iran.

Received 23 March 2019; received in revised form 10 August 2019; accepted 27 August 2019

ABSTRACT

The samples of spent chlorinated Pt/Al_2O_3 catalysts that were used in the isomerization process were decoked at elevated temperatures under airflow and different oxygen concentrations. The surface of the catalyst was characterized by thermal gravimetric analysis, differential scanning calorimetry, Brunauer-Emmett-Teller analysis, attenuated total reflection fast Fourier infrared spectroscopy, scanning electron microscopy and energy-dispersive X-ray elemental mapping. The effective parameters for the catalyst decoking optimized were coke burning temperature (450-600 ℃), temperature ramp (5-25 ℃/min) and oxygen content of the feed gas (0.5-2.0% *vol*.) in a tubular fixed-bed reactor using the response surface experimental design method. The spectroscopic tests were set based on the absorbance at 1390 cm^{-1}, representing the surface coverage of platinum-alumina, and the results revealed that the greatest safe regeneration of chlorinated Pt/Al_2O_3 catalyst is achieved under a specific concentration of oxygen, temperature domain and thermal ramp. Moreover, the mechanism and the reaction rates of the decoking step of the catalyst regeneration were examined and the kinetic parameters of chlorinated Pt/Al_2O_3 decoking were determined.

Keywords: *Catalyst fouling, Fixed-bed reactor, SEM mapping, Exothermic process, Catalyst deactivation, Regeneration.*

1. Introduction

Chlorinated Pt/Al_2O_3 catalyst due to its active sites and suitable porosity is used in a variety of chemical and catalytic processes such as isomerization [1,2], catalytic reforming [3], CO oxidation [4], propane and cyclohexane dehydrogenation [5,6] and hydrogenolysis of hexane [7]. What is remarkable is that the catalyst after long and frequent use will be deactivated and it should be regenerated for reuse. According to the reaction and process conditions, the lifetime of commercial chlorinated Pt/Al_2O_3 catalyst is assumed to be about 2 to 3 years [7].

This catalyst has an important and effective role in other industrial applications such as aromatization of heptane-2 [8], catalytic reforming of n-heptane [9] and dehydrogenation and oxydehydrogenation of paraffin [10]. The transformation of *n*-alkanes to *iso*-alkanes leading to increases in the octane number of gasoline is a process that has been catalyzed by chlorinated Pt/Al_2O_3 catalysts [11].

*Corresponding author.
E-mail address: hamed.abbasi1992@gmail.com (H. Abbasi)

In another study, the deactivation methods of chlorinated Pt/Al_2O_3 catalyst were realized and the appropriate methods were propounded to delay the catalyst deactivation. It was revealed that coke distribution on catalyst surfaces can determine the active sites and the catalyst activity [12].

Based on the operating conditions, the side reactions of the main process (such as polymerization, dehydrogenation, and condensation) intensify the coking phenomena on catalyst surfaces [12,13]. It was realized that at 100 ℃, the main precipitated components are carbonyl compounds (C=O) while olefinic and aliphatic compounds (C=C) were formed at higher temperatures. It was reported that chlorine-containing compounds reduce the amount of aromatic hydrocarbon deposits on the catalyst surface at 350 ℃. Zhorov and Ostrer [14] developed a catalyst regeneration process to remove 50% of coke and to return 80% of catalyst activity. A linear equation revealed the inverse relationship of coke content and active surface area in the above- mentioned catalyst [15].

Coke burning is an exothermic process, so it must be controlled to avoid the platinum agglomeration and

catalyst sintering. Decoking is carried out under airflow containing low levels of oxygen (0.5 to 2.0 vol. %) and at a temperature in the range of 400-600 ℃ to avoid sintering alumina [3,16]. Decoking of chlorinated Pt/Al_2O_3 was studied previously by extended X-ray absorption fine structure (EXAFS) [17], temperature programmed oxidation (TPO) and differential thermal analysis (DTA) [18]. Garetto and Apesteguia [19] determined the effect of the accessible metal fraction and the metal particle size on the coked chlorinated Pt/Al_2O_3 catalyst. Zanuttini [20] found that the amount of carbon formation on this catalyst is significantly related to the ratio of acidic sites to metal sites. Barbier [21] showed that at temperatures above 400 ℃, the amount of deposited coke increases with an increasing number of existing metal atoms. León et al. [22] predicted the composition of coke produced in vacuum residues by infrared spectroscopy.

Many studies have been carried out on the coke accumulation and adsorption of carbon monoxide on the Pt/Al_2O_3 catalysts by attenuated total reflection fast Fourier infrared spectroscopy (ATR-FTIR). Sato et al. [23] studied the adsorption and oxidation of CO on commercial nanoparticle catalysts supported on Pt/C, Pt_3Co/C, and PtRu/C. Koichumanova *et al.* [24] investigated the phase transformation of γ-Al_2O_3 into boehmite under the hydrothermal conditions of aqueous phase reforming.

Ortiz-Hernandez *et al.* [25] investigated acetonitrile adsorption in hexane on films of Pt/γ-Al_2O_3 deposited on a germanium waveguide. CO oxidation mechanisms on Pt/γ-Al_2O_3 catalyst were studied by Hongwei Gao [26]. FTIR characterization of chlorinated Pt/Al2O3 catalyst was performed and it was reported that at high dispersions of platinum, Pt-CO bands appeared at lower wavenumbers [27]. Likewise, CO adsorption was studied on Pt/CeO_2 [28], Pt–H–ZSM, Pt−Na−Mordenite, and $Pt/Rh/CeO_2/Al_2O_3$ catalysts respectively [29-31].

Jackson [32] examined the high-temperature adsorption of ethene, propene, propyne and carbon monoxide over nickel and platinum catalysts and it was concluded that hydrocarbons are adsorbed by platinum at the reduction step leading to appearance methylene and methyl signals at 2800 and 3000 cm^{-1}, respectively. Rivera-Latas *et al.* [33] studied the Pt surface covered with coke following the hydrogenolysis of hexane and they found out that platinum is very sensitive to poisoning by acetylene at the normal conditions for ethylene hydrogenation. A new approach for estimating the dispersion of Pt was developed through monitoring of CO adsorption over Pt/MFI catalyst [34].

In this paper, decoking conditions of chlorinated Pt/Al_2O_3 catalyst were studied and the effects of burning temperature, oxygen content, resident time and temperature ramp were examined and optimized by response surface methodology (RSM). The characteristic tests were performed by a specification of catalyst surfaces based upon the spectroscopic signals revealed both coke and platinum distribution. The mechanism of decoking, the reaction rates on the catalyst surfaces and the kinetic parameters were determined and reported. The outcomes were obtained using a rational design and analyzing the catalyst samples by a series of instruments such as TGA/DTA, DSC, BET, ATR-FTIR, EDX, SEM, as well as by RSM modeling. The novelty of this research is to achieve low-cost condition for this catalyst regeneration. Reducing process time and operating at lower temperatures reduce the cost of operation and depreciation of equipment.

2. Experimental

The spent spherical chlorinated Pt/Al_2O_3 catalyst pellets were extracted from the isomerization unit of a petroleum refinery (OD=6 mm). A Mass flow controller (model 5850s Brooks MFC) and a flowmeter (Agilent) were used for adjusting N_2 gas flow and checking the outlet gas flow, respectively. A stainless-steel tubular fixed bed reactor with the inner diameter of 10 *mm* and length of 20 *cm*, electric furnace with thermal programming capacity, ATR-FTIR spectrophotometer (Bruker Tensor 27), TGA/DSC analyzer (Mettler Toledo), BET sorption analyzer (Belsorp mini II) and scanning electron microscopy (Tescan Vega) were used. Fig. 1 illustrated the schematic of the experimental set-up.

The feed gases of air and nitrogen were regulated by needle valves and mass flow meters and were mixed by predetermined ratios. The mixed gas was directly fed to the reactor that was located at the furnace chamber. The effluent gas was exhausted from the reactor to an atmospheric mass flow meter.

2.1. Thermal Analysis

TGA was performed on the spent chlorinated Pt/Al_2O_3 catalyst using a TGA/DSC instrument (Mettler Toledo). The temperature of the catalyst samples was increased to 80 ℃ under dry nitrogen atmosphere by using a 10 °C/min ramp and remained at that temperature for 30 min. Then the catalyst was exposed to air at a flow rate of 100 cc/min and the temperature of the catalyst was increased to 600 ℃. The heat treatment pattern performed on the spent catalyst is shown in Fig. 2.

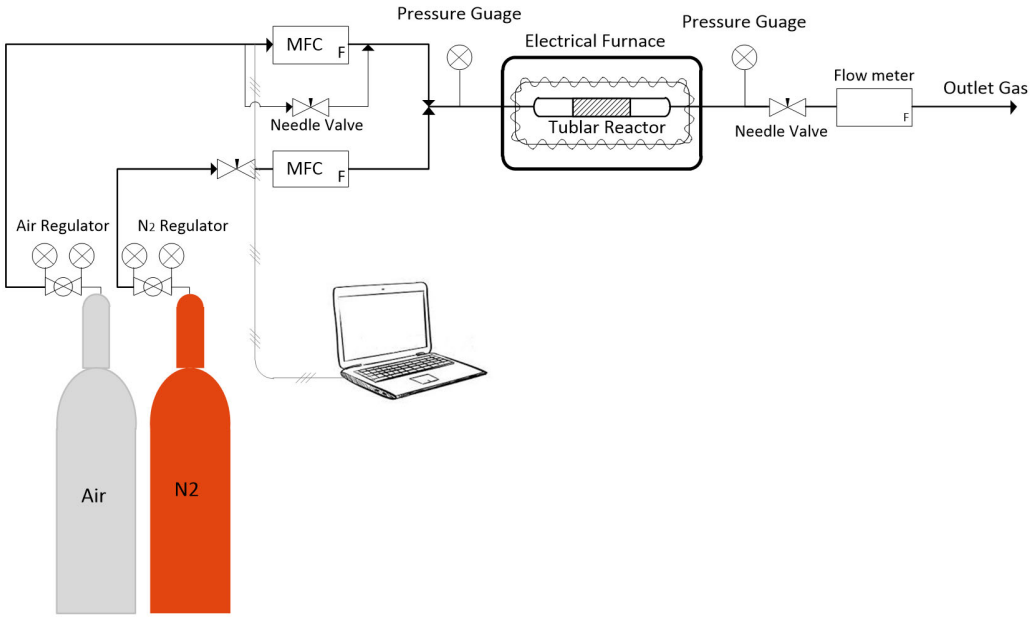

Fig. 1. Graphical illustration of experimental set-up.

By examining the TGA results shown in Fig. 2 it was revealed that at the temperature range of 80-100 °C, the sample weight of the catalyst decreased by 1.3% since the moisture content of the catalyst was removed due to heat absorption. A 5% reduction in sample weight was observed at the temperature range of 100-540 °C, which can be divided into two regions of 100-350 °C and 350-540 °C. In the first region, the volatile compounds that are present on the catalyst were combusted leading to a weight loss of 3% while another weight reduction of 1.2% was recorded in the temperature range of 350-540 °C due to the decomposition of the adsorbed hydrocarbons as well as the coke burning step. Then, carbon films that are strongly adsorbed by the catalyst surface are burned at the temperature range of 540-800 °C causing the sample weight to be decreased by 1.2% [35].

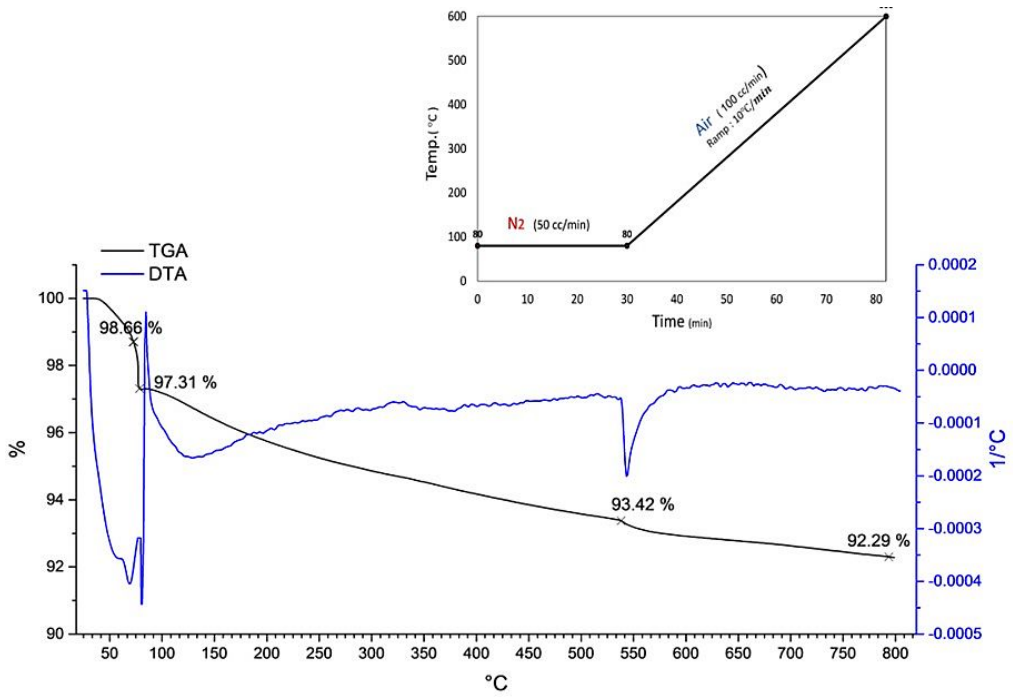

Fig. 2. TGA/DTA thermogram and the temperature pattern of chlorinated Pt/Al_2O_3 spent catalyst.

With DSC analysis, the temperature of the catalyst samples was ramped to 80 ℃ in dry nitrogen at a flow rate of 50 cc/min and a temperature ramp of 10 °C/min. It was left at that temperature for 30 minutes and then exposed to air until reaching 600 ℃. As shown in Fig. 3, an endothermic process occurs within the thermal range of 80-160 ℃. Given the proximity of this temperature to the evaporation temperature of the water, it can be said that the moisture content on the catalyst is evaporated by absorbing the heat at about 80 ℃, which leads to weight loss in this area. Finally, at 166 ℃, the water vapor is completely removed from the catalyst pores [36].

According to the DSC thermogram, the coke burning phenomena is classified into two steps. As shown in Fig. 3, first the amorphous and fibrous carbons begin to adsorb the high temperature oxygen molecules at 330-400 ℃ during an endothermic process until they reach the melting point. After oxygen uptake, the burning process begins and the energy level was increased at 400-480 ℃ since the coke burning was accompanied by heat-loss. After this step, the cokes that deposited on the catalyst surface with a stronger bond, begin to adsorb oxygen molecules and heat at 480-550 ℃ in other to be prepared for high-temperature burning. The temperature ranges indicated in the DSC thermogram are close to the temperature ranges in the TGA graph, and their results are consistent with each other.

2.2. Kinetics of coke burning

To determine the coke burning kinetics, the total conversion rate was calculated and drawn versus temperatures as shown in Fig. 4. Since the catalyst contained various types of coke as well as moisture and impurities, the conversion rate graph is divided into four parts as represented in Fig. 4.

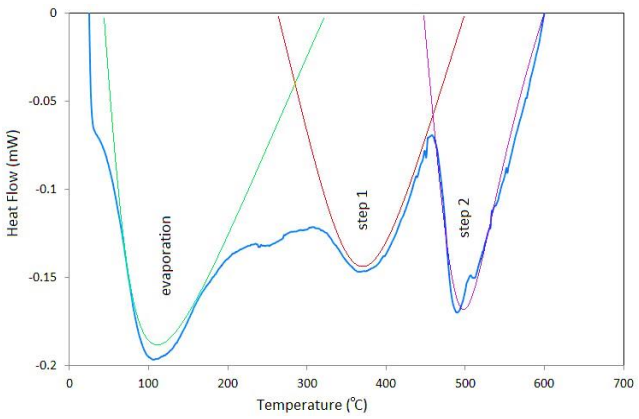

Fig. 3. The DSC curves of spent catalyst.

The kinetic parameters were determined for each section in a range of conversion values (0.1-0.9) to increase the validity of estimated kinetics.

At the constant temperature ramp of TG diagram, the Coats-Redfern method and Arrhenius's first order law were used to determine the kinetic parameters according to Eq. (1) [37]:

$$\frac{d\alpha}{dt} = A \cdot exp\left[-\frac{E}{RT}\right] \cdot f(\alpha) \quad (1)$$

$$\alpha = \frac{m_0 - m_t}{m_0 - m_\infty} \quad (2)$$

Where, α denotes the conversion rate; $f(\alpha)$ is the hypothetical model of the reaction mechanism, A shows the frequency factor (min^{-1}), E indicates the reaction activation energy (kj/mol), R is the gas constant (8.314 $J.mol^{-1}.K^{-1}$), m_0 is the initial weight of the sample; m_t is the sample weight at time t and m_∞ is the sample's final weight. When the temperature ramp ($\beta = \frac{dT}{dt}$) is constant, Eq. (3) is used and by assuming n=1, Eq. (5) is obtained [37].

$$\frac{d\alpha}{dt} = f(\alpha).\frac{A}{\beta} \cdot exp\left[-\frac{E}{RT}\right] \quad (3)$$

$$f(\alpha) = (1-\alpha)^n \quad (4)$$

$$ln\left|\frac{-ln(1-\alpha)}{T^2}\right| = ln\left[-\frac{AR}{\beta E}\left(1-\frac{2RT}{E}\right)\right] - \frac{E}{RT} \quad (5)$$

Now by plotting $\ln\left[\frac{-\ln(1-\alpha)}{T^2}\right]$ vs. $\frac{1}{T}$ and calculating the intercept and slope, it is possible to calculate the activation energy and frequency factor [37]. As shown in Fig. 5, this is done for all four sections and its results are reported in Table 1.

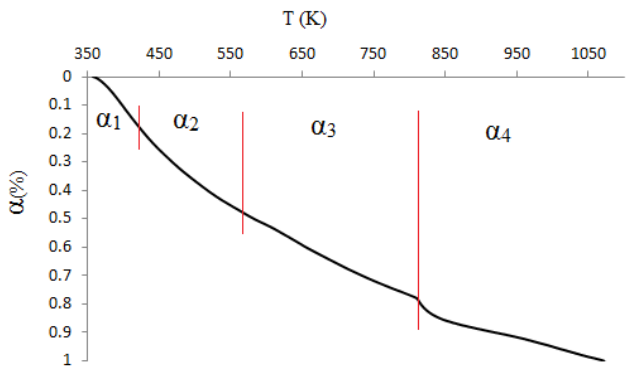

Fig. 4. The overall conversion rate of decoking process.

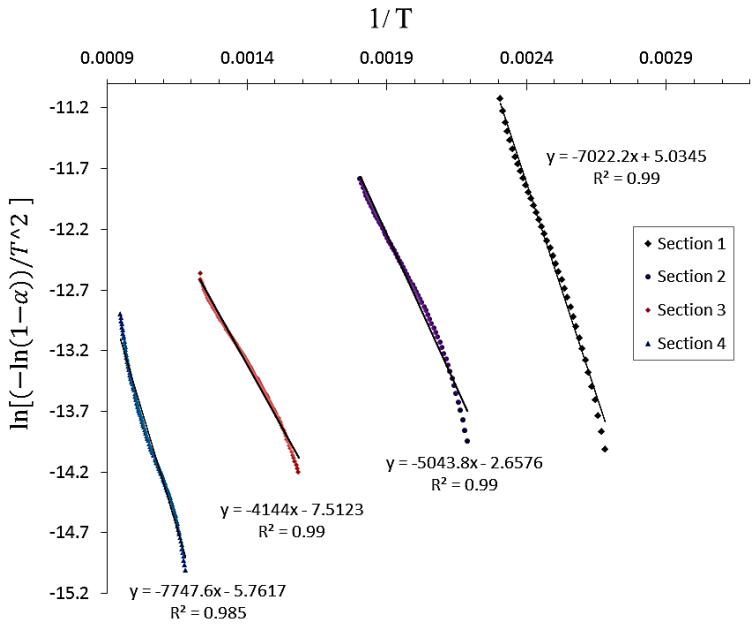

Fig. 5. Relationship of $\ln\left[\frac{-\ln(1-\alpha)}{T^2}\right]$ to $\frac{1}{T}$ for section 1 to 4.

Table 1. Kinetic parameters of coke combustion.

	$T_{average}$ (K)	Slop	Intercept	E (kJ/mol)	A (min^{-1})
section 1	433	-7022.2	5.03	58.38	1.22×10^{7}
section 2	505	-5043.8	-2.65	41.93	4.4×10^{3}
section 3	721	-4144	-7.51	34.45	34.7
section 4	951	-7747.6	-5.76	64.41	3.23×10^{2}

2.3. BET analysis

The Brunauer-Emmett-Teller (BET) theory and the Belsorp mini II sorption analyzer are used to estimate the specific surface area of the spent catalyst and its pore sizes. The absorption/desorption isotherm of the spent catalyst is shown in Fig. 6 and represents an isotherm of type IV, which is specific to the mesopore solid [38].

The BET theory is a conventional and common method for measuring the catalyst surface that is based on adsorption a gas such as N_2 on the catalyst surfaces for forming a monolayer (based on Langmuir isotherm) and allows calculating the surface area [39]. The BET diagram is shown in Fig. 7, the specific surface area, pore size, and total pore volume of the catalyst are calculated as 2.092 $m^2.g^{-1}$, 2.42 nm, and 0.0031 $cm^3.g^{-1}$ respectively and reported in Table 2. By comparing these values with the results of fresh Pt/Al_2O_3 catalyst that reported by Xiaohuin Liu and colleagues [40] in Table 2, it is observed that the surface area and the pore volume of the spent catalyst have been greatly reduced and this happened due to deposition of coke on the surface and catalyst pores.

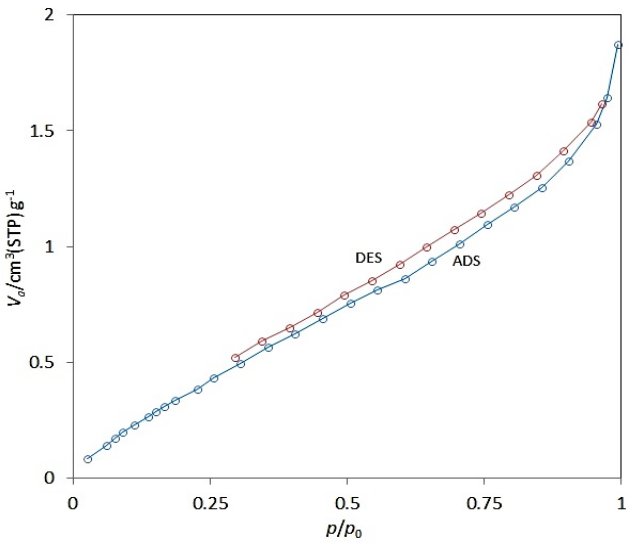

Fig. 6. Adsorption/desorption isotherm for the spent catalyst.

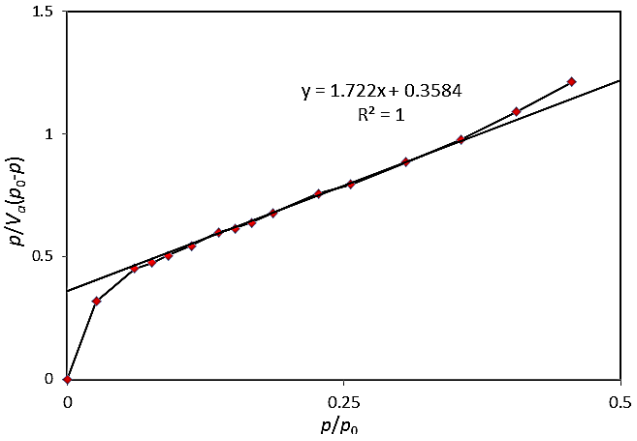

Fig. 7. BET diagram of the spent catalyst.

2.4. SEM-EDS analysis

To achieve the structure, the type and amount of catalyst constituent elements, the scanning electron microscope (SEM) and the energy-dispersive X-ray elemental mapping (EDS) analyses are carried out on the spent catalyst.

2.4.1. EDS analysis

As shown in Fig. 8, the spent catalyst contains chlorine, aluminum, oxygen, and carbon elements that most of these elements are aluminum and oxygen due to their presence in the catalyst support and platinum and chlorine have a lower percentage than other elements. Also, amounts of the coke obtained by using the catalyst in the chemical process are settled on it and cause the platinum particles to be covered with coke. The carbon signal is observed in Fig. 8.

2.4.2. SEM analysis

The SEM images of the spent catalyst in Fig. 9 show that particles on a scale of 250 to 500 nanometers are present at the catalyst surface. In Figs. 9(a) and 9(b), the black layer in some points of the catalyst surface especially on the catalyst support might be the coke accumulated on the catalyst surface. Figs. 9(c) and 9(d) show that the distribution and dispersion of particles is uniform. For example, the accumulation of compounds in the middle part of Fig. 9(d) is less than the corners.

Table 2. Comparison specific surface area, pore size and total pore volume of spent and fresh catalysts.

Characteristics	Spent catalysts	Fresh catalysts	Ref.
Total pore volume (cm^3g^{-1})	0.0031	0.32	[40]
Pore size (nm)	2.42	-	
Specific surface area (m^2g^{-1})	2.092	152.6	[40]

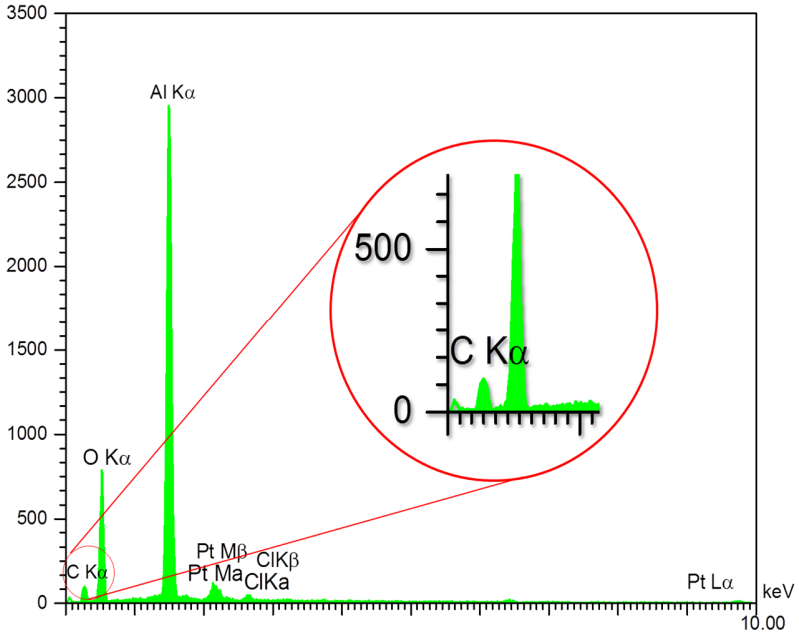

Fig. 8. EDS-mapping plot of chlorinated Pt/Al_2O_3 catalyst before decoking.

2.5. Decoking process

To regenerate the spent catalyst, it is necessary to perform decoking operations to remove the coke from the catalyst surface. Studies have shown that when the spent catalyst is subjected to thermal treatment, various parameters such as burning temperature and time, oxygen content, retention time at maximum temperature and temperature ramp are effective in this process.

As the results of TG and DSC analyses, it became clear that the burning of coke occurs at several stages, so the temperature is one of the parameters that influence the kinetics of this reaction and is therefore considered as one of the effective factors. Based on TG results, a temperature range of 450-600 ℃ is selected to study. Due to the exothermic nature of coke burning, the amount of oxygen intake as feed is also a controlling parameter of the decoking process because, with increasing oxygen content, the reaction speed is greatly increased and thus the possibility of sintering will increase. So, the percentage of oxygen in the feed must be very low to control the reaction.

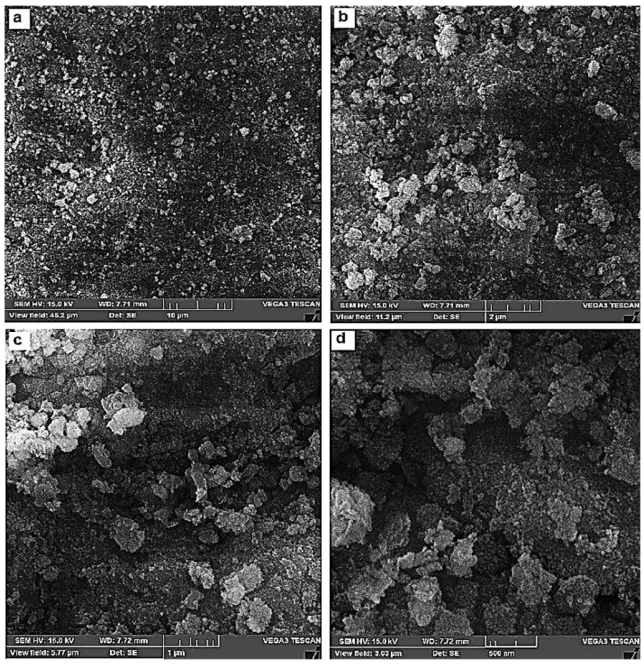

Fig. 9. SEM images of spent catalyst at (a) 10 µm, (b) 2.0 µm, (c) 1.0 µm and (d) 500 nm.

Table 3. Factors and levels of decoking stage.

Factors	A, O_2 content (%vol.)	B, Temperature ramp (°C/min)	C, Maximum temperature (°C)
Levels	0.5-2.5	5-25	450-600

Table 4. Decoking design of experiments by RSM.

Run	Factor A (% *vol*)	Factor B (°C/min)	Factor C (°C)
1	1.5	25	500
2	2	10	550
3	2	10	450
4	1.5	15	500
5	1.5	15	500
6	1.5	15	500
7	0.5	15	500
8	2	20	550
9	1	10	550
10	2	20	450
11	2.5	15	500
12	1	20	450
13	1	20	550
14	1.5	15	600
15	1.5	15	400
16	1.5	15	500
17	1.5	5	500
18	1	10	450

Therefore, this parameter is selected as an effective parameter. Based on the research, the range of 0.5-2 vol% is considered for the oxygen content of the feed gas. Also, since the burning and retention time at the desired temperature can be set by adjusting the temperature ramp, this factor is also chosen as the effective parameter at the decoking stage and the temperature ramp range is determined to be 5-25 ℃ based on the furnace capacity. Therefore, the three mentioned factors are chosen to examine their effect on the decoking stage. The factors along with their levels are presented in Table 3. The RSM method was used to design of experiments and achieve optimal conditions**.** The details are depicted in Table 4.

3. Results and discussion

This section reviews and analyzes the results in three sub-sections of determination of catalyst surface characteristics, design of experiment results and decoking optimization. In the first part, the results of ATR-FTIR analysis are investigated on the spent catalysts and then the effect of factors are analyzed on the spent catalysts and the decoking step is modeled. Finally, the optimization is done, and the values of the factors are determined to achieve optimal conditions and the necessary analyses are provided to confirm it.

3.1. Determination of catalyst surface characteristics

To perform quantitative and qualitative comparisons between samples of each experiment and spent catalyst and also decoking stage evaluation, the catalyst samples are studied by the ATR-FTIR method. In this analysis, the IR beam is radiated on catalyst samples and part of this beam is absorbed by matter and another part of it passes through it. Depending on the amount of beam passage and its reflection, each substance releases its unique infrared spectrum. Accordingly, using the position of these signals, the functional groups and the bonds in the sample can be determined [41, 45]. To ensure samples' homogeneousness, the catalyst samples are crushed and uniformed before the analysis. The ATR-FTIR analysis results of all 18 experiments are shown in Fig. 10. As shown in Fig. 10, there are three strong and distinct signals in the regions of 600-1000 cm^{-1}, 1000-1250 cm^{-1} and 3000-3750 cm^{-1} and four other poor signals are created in 1250-1400 cm^{-1}, 1500-1750 cm^{-1}, 2750-2850 cm^{-1} and 2850-3000 cm^{-1}.

As shown in Fig. 10, the catalysts contain functional groups such as CH_3, CH_2 and bonds such as C=C, C-H, C≡C, O-H, and C-O in their structure [46-49].

The strong signal in the region of 600-1000 cm^{-1} is related to the bond between the aluminum and the existing oxygen atoms (Al-O) at the support of the catalyst [40]. Because the catalyst is its support, this signal is stronger than other signals in the IR spectrum of the samples. The next strong signal in the region of ~1100 cm^{-1} indicates the bond between the carbons accumulated on the support of the catalyst and the oxygen atoms (C-O-C). During the decoking process, it is necessary to adsorb the oxygen initially, thus, this bond is generated during adsorption. The higher the amount of accumulated coke on the catalyst leads to a greater possibility of oxygen adsorption on the coke surface and therefore this signal will be stronger [46].

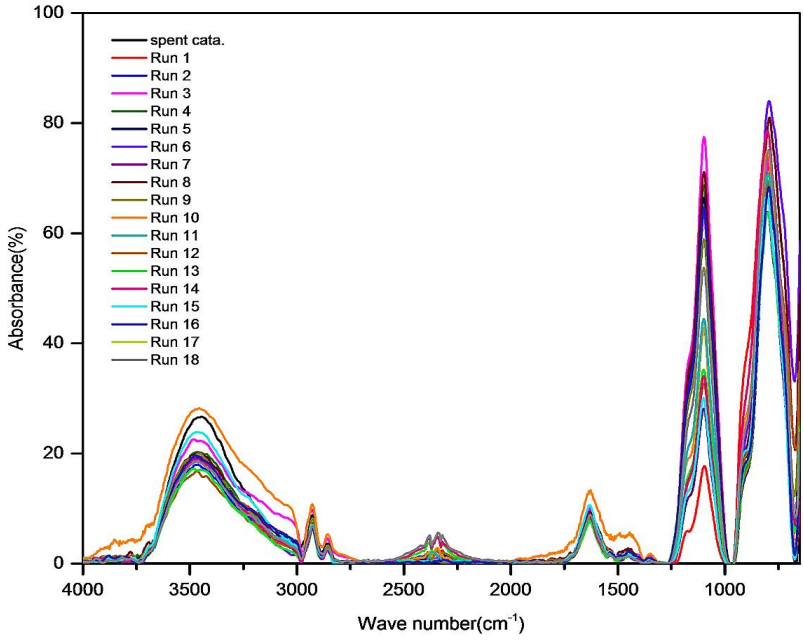

Fig. 10. All runs and spent catalyst ATR-FTIR peaks in 650-4000 cm^{-1}.

The weak signal at 1390 cm^{-1} is related to the bond between platinum atoms and the surface of the catalyst (Pt-O). Due to the fact that percentage of platinum in the catalyst structure is low (about 2%), and given that the catalyst surface is covered by carbon and coke, this signal is poor and has a short height. It is expected that by doing the decoking this bond and the strength of its related signal becomes clearer [50].

The bond between hydrogen and oxygen atoms (O-H) appears in two regions. The poor signal at 1600 cm^{-1} implies the presence of OH bond in water structure and the poor signal at 3400 cm^{-1} is related to the hydroxyl group in the support [23-25,46].

As shown in Fig. 10, three signals in the regions of 1460 cm^{-1}, 2850 cm^{-1} and 2930 cm^{-1} are observed which are due to the bond between the hydrocarbons present on the catalyst surface as well as the bond between the hydrogen and carbon atoms in the form of methyl and methylene groups. The IR bond at 2850 cm^{-1} belongs to the bond between carbon and hydrogen in the form of CH_2 and also the region of 2930 cm^{-1} is related to the bond between these atoms in the form of the methyl group (CH_3). One of the characteristics of these two signals is that they come immediately after each other and the height of the first signal (2850 cm^{-1}) is shorter than the second signal (2930 cm^{-1}) [46].

Signals relating to carbon monoxide (CO) and carbon dioxide (CO_2), which are often poor, are detected in 2100 cm^{-1} and 2300 cm^{-1} [27-33,51]. Of course, depending on the type of device used in ATR-FTIR analysis, the location of these signals varies slightly [34].

As shown in Fig. 10, the peak heights of 2850 and 2930 cm^{-1} are reduced in all experiments except for experiment 10 relative to the same position in the spent catalyst which indicates the reduction of methylene groups due to the burning of hydrocarbon compounds.

The highest decrease is also related to the experiment 13. But in experiment 13, the signal heights of 2850 cm^{-1} and 2930 cm^{-1} have increased relative to the spent catalyst, indicating an increase in methyl groups after decoking.

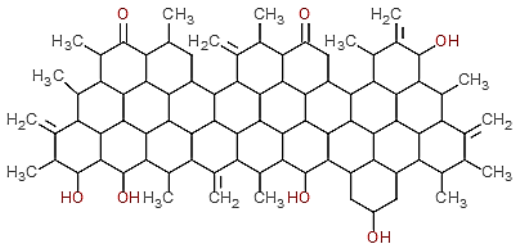

Fig. 11. Multilayer carbon schematic that covers catalyst surface and active sites.

The reason for this is that the burning of hydrocarbon compounds does not occur in a particular pattern. As shown in Fig. 11, due to the multi-layered hydrocarbon composition accumulated on the catalyst, it is possible that a layer of coke accumulated on the active metal or support surface burns out and other hydrocarbon compounds appear due to the separation of a layer of carbon from one part and migration to other parts of the catalyst. In fact, part of the coke burns out and releases in the form of carbon dioxide and carbon monoxide and the free radicals created by breaking the carbon rings cause the formation of the C-H bond in the form of groups such as methyl that the reconstructed image of this process is shown in Fig. 11 [46]. The ATR-FTIR spectra of the experiments 10 and 13 and the spent catalyst are shown separately in Fig. 12.

According to the above mentioned, despite burning coke, determination of the optimal best conditions and experiments for decoking is not possible based on peaks height of 2850 cm^{-1} and 2930 cm^{-1}.

Providing the surface of platinum is covered by coke and hydrocarbons, the vibration of Al-Pt becomes weak, but as soon as parts of the coke were accumulated on the metal burns, the peak related to the bond between platinum and catalyst support appears. The catalysis active sites on the catalyst structure are determined by vibrational signals of 1390 cm^{-1}. Therefore, an experiment that its peak height of 1390 cm^{-1} is higher in the ATR-FTIR graph of its samples could provide more active sites for catalytic processes. So, the peak height of 1390 cm^{-1} is selected as a measure of assessing the results of the experiments.

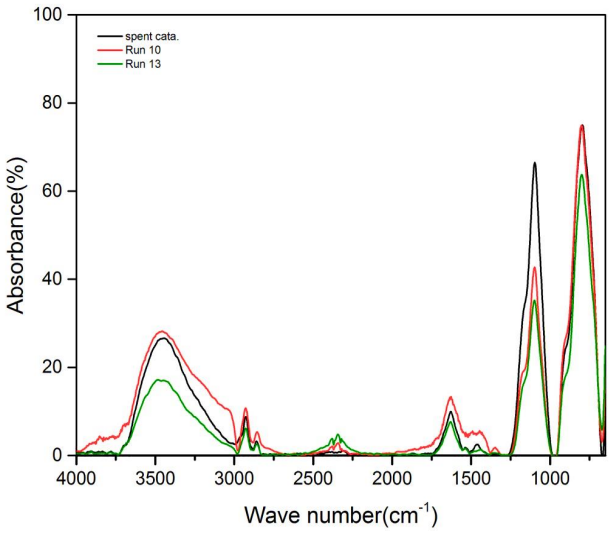

Fig. 12. Run numbers 3,5,10 and the spent catalyst ATR-FTIR graphs. Runs 3, 5 and 10 in regions 2850 and 2930 cm^{-1} have higher peaks than the spent catalyst.

3.2. Design of experiment results

To ensure the repeatability of the results, the analysis of each sample was repeated ten times. After ensuring the repeatability of the results, the signal height of 1390 cm^{-1} is entered into the Design Expert 10 software as a response. Then ANOVA (analysis of variance) was carried out and the results are presented in Table 5.

The best function that was in good agreement with the data and results is selected as the final model as Eq. (6).

$$(R + 0.15)^3 = +0.014+3.608E\text{-}003A+3.950E\text{-}003B - 4.056E\text{-}003\ C - 1.270E\text{-}003A\cdot B - 7.465E\text{-}003A\cdot C+7.034E\text{-}004B\cdot C \quad (6)$$

Where R shows the response (1390 cm^{-1} peak height), A is O_2 content (% vol.), B is maximum temperature ℃) and C shows the temperature ramp (°C/min). Based on ANOVA data the proposed model is consistent with the results and decoking temperature, the temperature ramp and oxygen content of feed gas have a significant effect on the results because their P-value is lower than 0.05 (95% confidence limit). Also, the interaction between the temperature (at which decoking takes place) and the oxygen content of the feed gas has a significant effect. Considering the effects of temperature on the molecular movement and the velocity of oxygen molecules, it can be concluded that the temperature influences the oxygen molecules penetration from the catalyst surface and reaching the coke accumulated in the catalyst and burning them.

As shown in Table 5, the predicted R-squared of the model is 0.82, which has a suitable agreement with the adjusted R-squared (0.71). The F-value of the obtained model (8.12) and the F-value of all three factors in this model are greater than $F_{6,17}$ and $F_{1,17}$ in the F-table ($F_{1,17\ Table} = 4.45$, $F_{6,17\ Table}=2.69$) with a confidence level of 95% indicating the significance of the factor effect on the results. The lack of fit was also greater than the pure error; this indicates a proper agreement between the predicted model and these data [52,53].

3.3. Optimizing the results

After investigating the effects of various factors on burning the catalyst coke, optimum conditions are determined for the decoking stage. To achieve the platinum metal maximum access, the signal height of 1390 cm^{-1} is considered as an optimization target.

These values can be matched to factor values in run 10. So, run 10 is assumed to depict the optimal conditions of decoking. Besides, due to the increased probability of sintering of the catalyst and alteration of the alumina phase at a temperature higher than 450 ℃, the predetermined conditions of decoking are assumed to be practical [20].

3.4. Determination of catalyst profile after optimization

3.4.1. EDS-mapping analysis

The EDS-mapping analysis is performed on the catalyst after the decoking process. The results of the EDS-mapping analysis in Fig. 13 show that the aluminum and oxygen elements have the largest share of elements due to their presence in the support (alumina) of the catalyst and considering that the support forms the main part of the catalyst. The spent catalyst is also used for reactions such as reforming and isomerization containing carbon and coke that the results Table 6 confirm the accuracy of this claim.

Table 5. ANOVA table for RSM results.

Source	Sum of Squares	df	Mean Square	F-Value	p-value Prob > F
Model	1.184E-003	6	1.973E-004	8.12	0.0016
A-O_2	2.082E-004	1	2.082E-004	8.58	0.0137
B-Rate	2.496E-004	1	2.496E-004	10.28	0.0084
C-max temp	2.632E-004	1	2.632E-004	10.84	0.0072
AB	1.289E-005	1	1.289E-005	0.53	0.4814
AC	4.458E-004	1	4.458E-004	18.36	0.0013
BC	3.958E-006	1	3.958E-006	0.16	0.6942
Residual	2.671E-004	11	2.428E-005	-	-
Lack of Fit	1.974E-004	8	2.467E-005	1.06	0.5355
Pure Error	6.973E-005	3	2.324E-005	-	-
Cor Total	1.451E-003	17	-	-	-

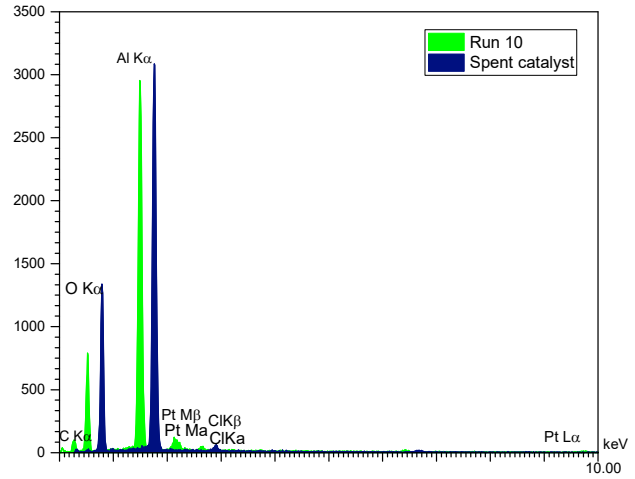

Fig. 13. EDS-mapping plot of chlorinated Pt/Al_2O_3 catalyst before and after decoking.

The EDS-mapping analysis of run 10 in Fig. 13 show that decoking results in the removal of carbon from the spent catalyst. Due to the use of oxygen at the decoking stage, part of it is used to burn hydrocarbon compounds and the other part reacts with other compounds found in the support; therefore, its amount is increased after decoking. Also, due to the removal of carbon from the catalyst surface, the chlorine atoms below the coke compounds appear after the removal of coke. Also, by decreasing the share of carbon, the proportion of chlorine is increased. The catalyst EDS plot before and after decoking are shown in Fig. 13.

3.4.2. BET analysis

Decoking has increased the specific surface area, pore size, and total pore volumes of the spent catalyst. Due to the burning of hydrocarbon compounds and coke accumulated at the catalyst surface and its pores, it is expected that the pores blocked by the coke get open and the access to platinum metal increase; the results are shown in Table 7 illustrate this issue and indicate that the specific surface area, pore size and total pore volume of the catalyst pore are 70, 8 and 175 times greater than before respectively.

Also as shown in Fig. 14, the absorption/desorption isotherm of catalyst samples after decoking, like the spent catalyst, is of type IV and related to the mesoporous solid [38]. Comparing these two graphs indicates that by performing the decoking process the absorption/desorption isotherms are not changed significantly.

4. Conclusions

The results and achievements of coke burning stage can be summarized as follows:

1. Analyzing the results of this study using ANOVA showed that the three factors of the coke burning temperature, the temperature ramp, the amount of oxygen gas in the feed and the interaction between the burning temperatures, have a significant effect on the coke burning process due to the effect of temperature on the velocity of gases and consequently improve the mass transfer when the coke burning has the highest and the amount of oxygen gas in the feed has the lowest effect on coke burning.

2. The coke burning stage follows a third-order power model and when the factors are set to the following values, it is possible to achieve the optimum coke burning performance. (1) Coke burning temperature = 450 ℃, (2) The temperature ramp =20 $^{\circ}$C/min and (3) Oxygen content = 2 vol%.

3. Due to the difference in the type of carbon found on the catalyst surface, the coke burning of the hydrocarbons accumulated on the catalyst occurs in two regions of 330-400 ℃ and 450-550 ℃.

By burning the cokes that have covered the platinum surface and blocked the catalyst pores, the specific surface area, pore size and total pore volume of the catalyst are 70, 8 and 176 times greater than before, respectively and the carbon content of the catalyst is significantly reduced.

Table 6. Quantitative result of EDS analysis for the spent catalyst and run 10.

Run 10 (w%)	Spent catalyst (w %)	Elements
54.38	55.62	Al
40.26	24.3	O
3.03	9.65	Pt
0	9.58	C
2.33	0.85	Cl

Table 7. Comparison specific surface area, pore size and total pore volume before and after decoking.

Step	Total pore volume ($cm^3.g^{-1}$)	d_{pore} (nm)	$a_{s, BET}$ ($m^2.g^{-1}$)
Before decoking	0.0031	2.42	2.092
After decoking	0.5454	16.04	140.3

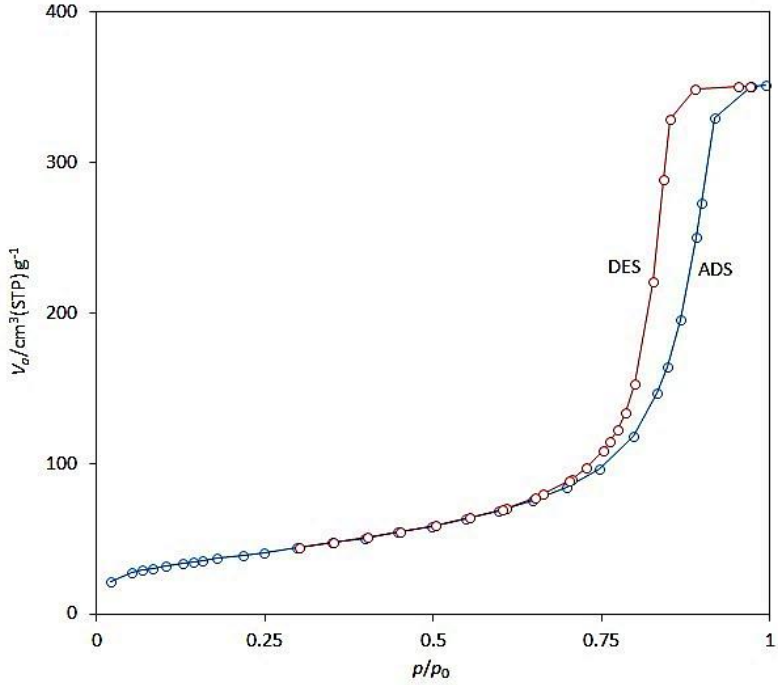

Fig. 14. Chlorinated Pt/Al_2O_3 catalyst adsorption/desorption isotherm after coke burning.

References

[1] J. Hidalgo, M. Zbuzek, R. Černý, P. Jíša, Open Chem. 12 (2014) 1–13.

[2] F. Garin, S. Aeiyach, P. Legare, G. Maire, J. Catal. 77 (1982) 323–337.

[3] M. P. Lapinski, S. Metro, P. R. Pujadó, M. Moser, Catalytic Reforming in Petroleum Processing, in Handbook of Petroleum Processing, Springer International Publishing, 2015, 229–260.

[4] A. Manasilp, E. Gulari, Appl. Catal. B 37 (2002) 17–25.

[5] F. Jiang, L. Zeng, S. Li, G. Liu, S. Wang, J. Gong, ACS Catal. 5 (2015) 438–447.

[6] R. W. Maatman, P. Mahaffy, P. Hoekstra, C. Addink, J. Catal. 23 (1971) 105–118.

[7] C. Corolleur, J. Catal. 24 (1972) 385-400.

[8] F. Aberuagba, React. Kinet. Catal. Lett. 70 (2000) 243–249.

[9] J. Beltramini, D. L. Trimm, Appl. Catal. 31 (1987) 113-118.

[10] M. Bhasin, J. McCain, B. Vora, T. Imai, P. Pujadó, Appl. Catal. A 221 (2001) 397–419.

[11] D. Mei, J. H. Kwak, J. Hu, S. J. Cho, J. Szanyi, L. F. Allard, C. H. F. Peden, J. Phys. Chem. Lett. 1 (2010) 2688–2691.

[12] J. Moulijn, A. van Diepen, F. Kapteijn, Appl. Catal. A 212 (2001) 3–16.

[13] Z. Sarbak, in: E. G. Derouane, V. Parmon, F. Lemos, F. Ramôa Ribeiro, (Eds.), Coke formation on alumina and alumina supported platinum catalysts, in sustainable strategies for the upgrading of natural Gas: fundamentals, challenges, and opportunities, Springer-Verlag, Berlin, 2005, pp. 359–364.

[14] Y. M. Zhorov, L. A. Ostrer, Chem. Technol. Fuels Oils. 26 (1990) 226–229.

[15] A. G. Gayubo, F. J. Lorens, E. A. Cepeda, J. Bilbao, Ind. Eng. Chem. Res. 36 (1997) 5189–5195.

[16] M. Argyle, C. Bartholomew, Catalysts 5 (2015) 145–269.

[17] F. Le Normand, A. Borgna, T. F. Garetto, C. R. Apesteguia, B. Moraweck, J. Phys. Chem. 100 (1996) 9068–9076.

[18] B. B. Zharkov, V. L. Medzhinskii, L. F. Butochnikova, O. M. Oranskaya, V. B. Maryshev, Chem. Technol. Fuels Oils. 24 (1988) 157–159.

[19] T. F. Garetto, C. R. Apesteguia, Appl. Catal. 20 (1986) 133–143.

[20] M. S. Zanuttini, M. A. Peralta, C. A. Querini, Ind. Eng. Ch em. Res. 54 (2015) 4929–4939.

[21] J. Barbier, Appl. Catal. 23 (1986) 225–243.

[22] A. Y. León, N. A. Rodríguez, E. Mejía, R. Cabanzo, J. Phys. Conf. Ser. 687 (2016) 012092.

[23] T. Sato, K. Kunimatsu, M. Watanabe, H. Uchida, J. Nanosci. Nanotechnol. 11 (2011) 5123–5130.

[24] K. Koichumanova, K. B. Sai Sankar Gupta, L. Lefferts, B. L. Mojet, K. Seshan, Phys. Chem. Chem. Phys. 17 (2015) 23795–23804.

[25] I. Ortiz-Hernandez, D. Jason Owens, M. R. Strunk, C. T. Williams, Langmuir 22 (2006) 2629–2639.

[26] H. Gao, Appl. Surf. Sci. 379 (2016) 347–357.

[27] G. J. Arteaga, J. A. Anderson, C. H. Rochester, Catal. Lett. 8 (1999) 189–194.

[28] P. Bazin, O. Saur, J. C. Lavalley, M. Daturi, G. Blanchard, Phys. Chem. Chem. Phys. 7 (2005) 187-194.

[29] M. Mihaylov, K. Chakarova, K. Hadjiivanov, O. Marie, M. Daturi, Langmuir 21 (2005) 11821–11828.
[30] K. Chakarova, M. Mihaylov, K. Hadjiivanov, Microporous Mesoporous Mater. 81 (2005) 305–312.
[31] T. Chafik, O. Dulaurent, J. L. Gass, D. Bianchi, J. Catal. 179 (1998) 503–514.
[32] S. David Jackson, N. Hussain, A. Shona Munro, J. Chem. Soc. Faraday Trans. 94 (1998) 955–961.
[33] F. J. Rivera-Latas, R. A. D. Betta, M. Boudart, AIChE J. 38 (1992) 771–780.
[34] N. S. Nesterenko, A. V. Avdey, A. Y. Ermilov, Int. J. Quantum Chem. 106 (2006) 2281–2289.
[35] H. Seo, J. K. Lee, U. G. Hong, G. Park, Y. Yoo, J. Lee, H. Chang, I. K. Song, Catal. Commun. 47 (2014) 22–27.
[36] H. M. Gobara, R. S. Mohamed, F. H. Khalil, M. S. El-Shall, S. A. Hassan, Egypt. J. Pet. 23 (2014) 105–118.
[37] G. Wang, J. Zhang, J. Shao, H. Ssun, H. Zuo, J. Iron Steel Res. Int. 21 (2014) 897–904.
[38] S. Lowell, J. E. Shields, Powder Surface Area and Porosity, Springer, Netherlands, 1991.
[39] M. Naderi, "Surface Area: Brunauer–Emmett–Teller (BET)." Progress in filtration and separation. Academic Press, 2015, pp. 585-608.
[40] X. Liu, Y. Guo, W. Xu, Y. Wang, X. Gong, Y. Guo, G. Lu, Kinet. Catal. 52 (2011) 817–822.
[41] J. O. Alben, F. G. Fiamingo, Fourier Transform Infrared Spectroscopy, Academic, New York, 1984, pp. 133–179.
[42] D. C. Harris, M. D. Bertolucci, Symmetry and Spectroscopy: An Introduction to Vibrational and Electronic Spectroscopy, Dover, 1978.
[43] R. Mehrotra, Infrared Spectroscopy, Gas Chromatography/Infrared in Food Analysis, in Encyclopedia of Analytical Chemistry, Chichester, UK, John Wiley & Sons, 2000.
[44] Z. Wu, Y. Zhao, J. Zhang, Y. Wang, Molecules 22 (2017) Article ID 1238.
[45] M. Morita, A. Yasuhara, Electron microscope and elemental mapping image generation method, US Pat. (2017) 9627175B2.
[46] D. L. Pavia, G. M. Lampman, G. S. Kriz, J. A. Vyvyan, Introduction to Spectroscopy, Cengage Learning, 2008.
[47] B. E. Obinaju, F. L. Martin, Environ. Int. 89–90 (2016) 93–101.
[48] J. Coates, Interpretation of Infrared Spectra, A Practical Approach, in Encyclopedia of Analytical Chemistry, Chichester, John Wiley & Sons, 2006.
[49] S. Alexander, V. Gomez, A. R. Barron, J. Nanomater. 2 (2016) 1–8.
[50] S. D. Ebbesen, B. L. Mojet, L. Lefferts, Langmuir 24 (2008) 869–879.
[51] D. Ferri, T. Bürgi, A. Baiker, J. Phys. Chem. B 105 (2001) 3187–3195.
[52] F. Yaripour, Z. Shariatinia, S. Sahebdelfar, A. Irandoukht, Fuel 139 (2015) 40–50.
[53] D. C. Montgomery, Design and Analysis of Experiments, John Wiley & Sons, Incorporated, 2017.
[54] D. L. Trimm, Introduction to Catalyst Deactivation, in J. L. Figueiredo (ed.), Progress in Catalyst Deactivation, Martinus Nijhoff Publishers, The Hague, 1982, pp. 3–22.